Thermal evolution of ZnO-Bi_2O_3-Sb_2O_3 system in the region of interest for varistors

M. PEITEADO*, M. A. DE LA RUBIA, J. F. FERNÁNDEZ, A. C. CABALLERO
Departamento de Electrocerámica, Instituto de Cerámica y Vidrio, CSIC, Madrid, 28049, Spain
E-mail: peitead@icv.csic.es

Published online: 3 March 2006

In facing the design of new processing strategies for ZnO based ceramic varistors, a precise control of its microstructural development during sintering is demanded. Addition of dopants to zinc oxide results in the formation of secondary phases that to a large extent determine the macroscopic electrical properties of the ceramic. In a varistor system based on ZnO with small additions of Bi_2O_3 and Sb_2O_3 these three oxides govern the reactions at high temperature that give place to the secondary phases. These reactions become then the head point from which the functional microstructure is configured. In this way the present work deals with the thermal evolution of the ZnO-Bi_2O_3-Sb_2O_3 system in the region of interest for varistors, revealing the existence of two simultaneous reactions paths during sintering these ceramics.

1. Introduction

ZnO-Bi_2O_3-Sb_2O_3 (ZBS) based varistors are electroceramic devices which exhibit highly nonlinear current-voltage characteristics that make them suitable for protecting against transient voltage surges [1–3].The non-ohmic behaviour is strongly related with the polycrystalline microstructure, in which ZnO grains separated by electrically active grain boundaries represent the majority phase [4–6]. Together with zinc oxide particles of a $Zn_7Sb_2O_{12}$ spinel type phase, as well as a continuous interconnected bismuth rich phase that percolates through the whole ceramic body are also common in ZBS varistors. The presence of a very thin Bi-rich amorphous film (1–2 nm) or intergranular segregation of Bi atoms at ZnO/ZnO grain boundaries contributes to the formation of potential barriers to electrical conduction in the vicinity of ZnO interfaces, which are responsible for the device nonlinearity [7–9]. Moreover depending on the composition, a small amount of a pyrochlore phase can also form [10].

Ceramic varistors are produced by sintering zinc oxide powders with small amounts of metal oxides such as Bi_2O_3, Sb_2O_3, CoO, MnO, Cr_2O_3, etc. As a result of the heating treatment, several thermally activated processes give place to chemical reactions between the varistor components that will lead to the different crystalline phases [3, 6]. The definite composition of the microstructure is therefore dependent on the existence and evolution of such reactions during sintering, and the selection of a proper sintering strategy becomes decisive to achieve a microstructure with the desired electrical properties [11]. For example the varistor *breakdown voltage*, i.e., the onset voltage magnitude of nonlinear conduction, is directly proportional to the average size of ZnO grains [2, 12]; hence the need for a controlled microstructural development which could be attained trough carefully controlling the sintering reactions. In a varistor system with ZnO, Bi_2O_3 and Sb_2O_3 these three oxides govern the reactions at high temperature. It was on 1975 when Wong first suggested a possible sequence of reactions implying the formation of a pyrochlore type compound of formula $Bi_2(Zn_{4/3}Sb_{2/3})O_6$ [13]. At higher temperatures this phase reacted with ZnO, readily available from bulk matrix, to form a spinel type compound as well as a Bi-rich liquid phase; bismuth oxide in the pyrochlore was totally replaced by an equivalent amount of ZnO without disturbing the $(Zn_{4/3}Sb_{2/3})$ sublattice:

$$Bi_2(Zn_{4/3}Sb_{2/3})O_6 + ZnO \xrightarrow{\Delta'} Zn(Zn_{4/3}Sb_{2/3})O_4 + Bi_2O_3(liq) \quad (1)$$

The presence of the liquid phase promotes densification as well as ZnO grain growth whereas the spinel phase is reported to act as grain growth inhibitor [4, 5]. Later in 1980 Inada proposed a similar sequence of reactions in

*Author to whom all correspondence should be addressed.
0022-2461
DOI: 10.1007/s10853-006-7168-5

the ternary system [14]:

$$2ZnO + 3/2Bi_2O_3 + 3/2Sb_2O_3 + 3/2O_2 \xrightarrow{<900^\circ C} Zn_2Bi_3Sb_3O_{14} \quad (2)$$

$$2Zn_2Bi_3Sb_3O_{14} + 17ZnO \xrightarrow{900^\circ C \sim 1050^\circ C} 3Zn_7Sb_2O_{12} + 3Bi_2O_3(liq) \quad (3)$$

According to Inada, reaction (3) was reversible on cooling although the presence of certain dopants like Cr, Mn, Co or Ni, tend to stabilize the spinel phase preventing its decomposition to pyrochlore. There was however a disagreement in the pyrochlore chemical composition proposed by Inada from that suggested by Wong. Prevalence of the first one was revealed in 1989 by Kim *et al*. [15] and recently confirmed by Mergen & Lee (1997) [16]. Kim reports on ZnO-Sb_2O_3, ZnO-Bi_2O_3 and ZnO-Sb_2O_3-Bi_2O_3 varistor systems showed that densification is strongly related to the formation of pyrochlore and the liquid phases, and this is restrained to the Sb/Bi relationship. Being $Sb_2O_3/Bi_2O_3 = 1$ the Sb/Bi ratio that corresponds to the pyrochlore stoichiometric formulation, relations greater than unity give place to liquid formation around 740°C as a result of the eutectic interaction between ZnO and Bi_2O_3 [15, 17]; on the other hand, Sb/Bi ratios smaller than 1 delay liquid appearance to higher temperatures, until the decomposition of pyrochlore (reaction 3).

In the earlier nineties Olsson studies about the influence of dopants, sintering temperature, and heating and cooling rates on varistor microstructural development [5], suggested the existence of an additional reaction that come to explain the increase in spinel volumetric fraction for Sb/Bi relations greater than 1. In 1996 Leite *et al*. proposed then the following set of reactions [18]:

$$Sb_2O_3 + O_2 \xrightarrow{527^\circ C} Sb_2O_5(liq) \quad (4)$$

$$Sb_2O_5(liq) + ZnO \xrightarrow{700^\circ C \sim 850^\circ C} ZnSb_2O_6(s) \quad (5)$$

$$ZnSb_2O_6 + 6ZnO \xrightarrow{>800^\circ C} Zn_7Sb_2O_{12}(s) \quad (6)$$

$$3ZnSb_2O_6 + 3Bi_2O_3(s) + ZnO \xrightarrow{700^\circ C < T < 900^\circ C} Zn_2Bi_3Sb_3O_{14} \quad (7)$$

On the basis of previous works by Kim *et al*. [19] and Krasevec *et al*. [20] which suggested a mechanism of vaporization-condensation of antimony oxide around 500°C, Leite proposed with these reactions that Sb (III) first oxidizes to Sb_2O_5, liquid at this temperature; the pentoxide then goes into vaporization and further condensation over ZnO solid particles where it forms and intermediate $ZnSb_2O_6$ tri-rutile type phase. Such phase, whose existence was previously mentioned by Kim *et al*. and Inada himself, reacts then with the adjacent ZnO to straight form the spinel phase or either with ZnO and Bi_2O_3 to form pyrochlore which later transforms into spinel (reaction 3). Nevertheless the presence of antimony oxide (V) is subject of controversy as this compound decomposes roughly at 380°C releasing oxygen. More recently Ott *et al*. [21] as well as Kumari *et al*. [22] rejected this assumption and rewrote reactions (4) and (5) in the following way:

$$ZnO + Sb_2O_3 + O_2 \xrightarrow{600^\circ C < T < 800^\circ C} ZnSb_2O_6 \quad (8)$$

Ott and co-workers pointed out however that the presence of the $ZnSb_2O_6$ phase is unclear since the straight reaction could explain itself the additional formation of spinel [21]

$$7ZnO + Sb_2O_3 + O_2 \xrightarrow{>800^\circ C} ZnSb_2O_{12} \quad (9)$$

This possibility was refuted by Kumari who proposed the following route in the ZnO-Sb_2O_3 binary system [22]:

$$ZnO + Sb_2O_3 + O_2 \xrightarrow{>600^\circ C} ZnSb_2O_6 \xrightarrow[ZnO]{>800^\circ C} Zn_{2.33}Sb_{0.67}O_4 \quad (10)$$

$$Zn_{2.33}Sb_{0.67}O_4 \xrightarrow{>900^\circ C} Zn_7Sb_2O_{12} \quad (11)$$

Where $Zn_{2.33}Sb_{0.67}O_4$ (= $Zn_{6.99}Sb_{2.01}O_{12}$) is a non-stoichiometric compound that already possesses the spinel structure but with a cubic symmetry instead of that orthorhombic of the stoichiometric $Zn_7Sb_2O_{12}$. Transformation between both spinel phases could be avoided once again in presence of certain soluble dopants.

Reactions (1) to (11) are some of the proposals in literature to explain the varistor microstructural evolution during sintering. The absence of an accurate description of the whole process is the aim of this paper, focused primarily on thermal evolution of ZBS system but also on that of the pyrochlore and spinel intermediate phases and the pure oxides themselves.

2. Experimental

Progress with temperature of the different reactions in the ZBS system was studied over three different compositions in the region of interest for varistors. This implies molar percentages of ZnO above 95% but also Sb/Bi ratios greater than 1, i.e., no liquid phase should be present until the pyrochlore starts to decompose. Conventional solid state route was employed in which reagent grade oxides were mixed thoroughly including previous ball-milling for 2 hours in ethanol. First composition labelled A contains 98 % mol ZnO, 0.5 % Bi_2O_3 and 1.5 % Sb_2O_3 so that Sb/Bi ratio is equal to 3. Composition B involves a slight increase in the Bi_2O_3 amount as well as a decrease in that of the Sb_2O_3 with the subsequent decrease in the Sb/Bi

TABLE I Experimental compositions prepared to study the progress of the chemical reactions during sintering of ZnO-Sb_2O_3-Bi_2O_3 based varistors

	ZnO	Sb_2O_3	Bi_2O_3	Sb/Bi
Comp. A	98.0	1.5	0.5	3
Comp. B	98.0	1.2	0.8	1.5
Comp. C	98.0	1.8	0.2	9
$Zn_7Sb_2O_{12}$	87.5	12.5	–	–
$Zn_2Bi_3Sb_3O_{14}$	40	30	30	–

ratio, while in composition C the total amount of Bi_2O_3 is the smallest one of the three starting powders, and the Sb_2O_3 amount is the highest one. The three compositions as well as the Sb/Bi ratios are outlined in Table I.

Stoichiometric pyrochlore and spinel type compounds were individually prepared from the corresponding oxides (Table I). These two stoichiometric mixtures, the above mentioned compositions and the pure oxides themselves were heated to different temperatures ranging from 500 to 1050°C with a constant heating rate of 3°C min^{-1}. Once the temperature was achieved, samples were held for 5 minutes (labelled 0 hours) and for 72 hours soaking time and then rapidly quenched in air to avoid reactions and possible phase transformations on cooling. After quenching the calcined samples were grounded for characterization. Phase evolution was followed by X-Ray Diffraction in a D5000 Siemens diffractometer with a fully computerized Kristalloflex 710 generator using CuKα_1 radiation and Ni filter. The studied systems were also characterized by simultaneous Differential thermal analysis and Thermogravimetry (DTA/TG model 409 STA Netzsch) heating up in air to 1180°C and with a heating rate of 3°C min^{-1}. Finally Scanning Electron Microscopy coupled with Energy Dispersed Spectroscopy (SEM-EDS) was also carried out to analyse the microstructure of calcined samples in a Field Emission Hitachi S-4700 FE-SEM microscope.

3. Results and discussion

3.1. Pure oxides

No phase transformations are observed in pure zinc oxide (m.p. ∼1975°C; JCPDS File No. 36-1451) for the temperature range used in sintering ZnO-based varistors. In pure Bi_2O_3 two endothermic transformations take place, one around 730°C corresponding to the α-monoclinic (JCPDS File No. 41-1449) to δ-cubic transformation (JCPDS File No. 45-1344), and another one at 825°C which corresponds to the melting. With regard to the antimony oxide two polymorphs are known, cubic senarmontite (JCPDS File No. 75-1565) up to 600°C and orthorhombic valentinite (JCPDS File No. 11-0689) from 600°C to its melting at 655°C, although this behaviour changes in air because it takes place the oxidation of Sb_2O_3 around 500–530°C. Fig. 1 shows the results of DTA/TG analysis for pure Sb_2O_3; an exothermic peak at 520°C is clearly observed in DTA curve, together with a weight profit of ∼ 5% detected in the thermogravimetry test. The theoretical calculations however indicate that this weight gain actually corresponds to a partial oxidation of Sb (III) to the $Sb^{III}Sb^{V}O_4$ cervantite (JCPDS File No. 71-0564). Later annealing in air only promotes the decomposition of this α-Sb_2O_4 orthorhombic polymorph above 1050°C but without any further oxidation (Fig. 1). Its presence instead of the pentoxide is also confirmed by XRD in Fig. 2.

DTA/TG results for pure $Zn_7Sb_2O_{12}$ spinel type phase (Fig. 5) are quite similar to those of the pyrochlore mixture, with an oxidation process of Sb (III) that goes on after the formation of Sb_2O_4. There is however a slight different between both species, the smooth exothermic increase between 700 and 900°C observed in DTA curve

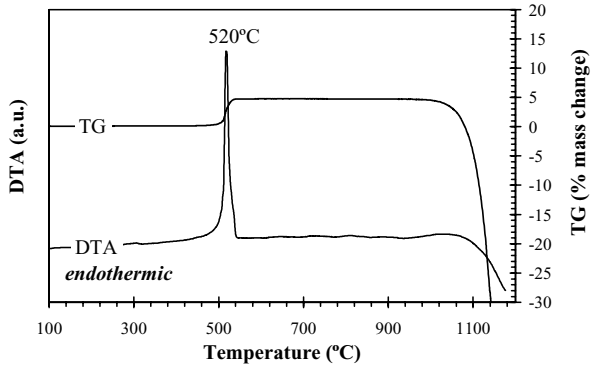

Figure 1 DTA/TG curves for pure Sb_2O_3 (heating rate 3°C/min).

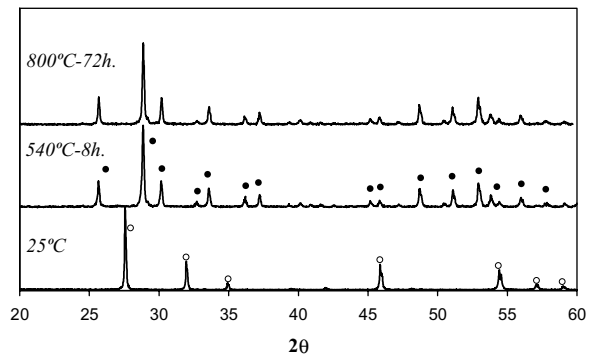

Figure 2 XRD patterns for pure Sb_2O_3 at different thermal treatments (quenched samples). White circles represent those peaks corresponding to the cubic Sb_2O_3 phase; black ones to the orthorhombic Sb_2O_4.

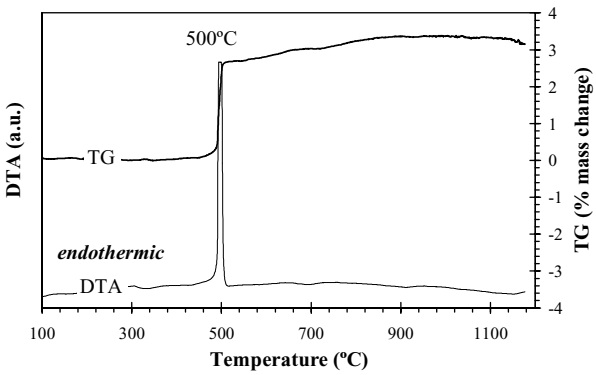

Figure 3 DTA/TG curves for $Zn_2Bi_3Sb_3O_{14}$ pyrochlore stoichiometric mixture.

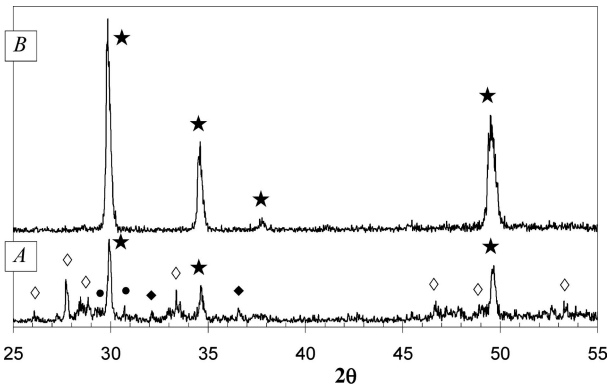

Figure 4 XRD patterns for $Zn_2Bi_3Sb_3O_{14}$ pyrochlore mixture. A) 530°C−0h. B) 950°C-0h. ♦ ZnO, ◊ Bi_2O_3, • Sb_2O_4, ⋆ $Zn_2Bi_3Sb_3O_{14}$.

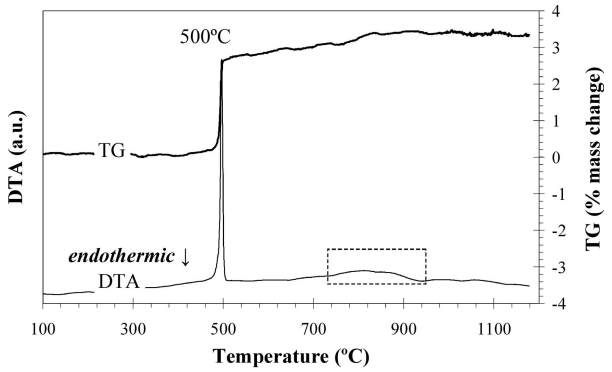

Figure 5 DTA/TG curves for $Zn_7Sb_2O_{12}$ spinel stoichiometric mixture.

of the spinel mixture (Fig. 5). Thermal treatments for 0 hours soaking time show that Sb_2O_4 slowly reacts with temperature and it is only since 900°C when the first peaks of a new compound are registered: the tetragonal $ZnSb_2O_6$ tri-rutile type phase (JCPDS File No. 38-453) (Fig. 6). No signals of spinel species are however detected in these essays, which should be attributed to kinetic restrictions of the involved processes. Such restrictions could be avoided when increasing the dwell time (4 hours before quenching) so that peaks of the tri-rutile phase as well as of a non-stoichiometric cubic $Zn_{2.33}Sb_{0.67}O_4$ spinel phase (JCPDS File No. 15-687) are already detected since 500°C (Fig. 7). The system goes on reacting and is above 1000°C when peaks of the orthorhombic stoichiometric $Zn_7Sb_2O_{12}$ spinel phase (JCPDS File No. 36-1445) are clearly observed. In this way, the exothermic increase at 700–900°C in DTA of Fig. 5 should be associated with the different transformations between Sb_2O_4, $ZnSb_2O_6$ and the two spinel structures.

3.2. Stoichiometric pyrochlore and spinel type compounds

Fig. 3 shows DTA/TG results for pure $Zn_2Bi_3Sb_3O_{14}$ pyrochlore. Again only one exothermic peak is observed by DTA around 500°C. The absence of more signals in this curve clearly indicates that formation of pyrochlore starts once the oxidation of antimony (III) has begun. However the TG detects a weight profit prolonged until 950°C, this

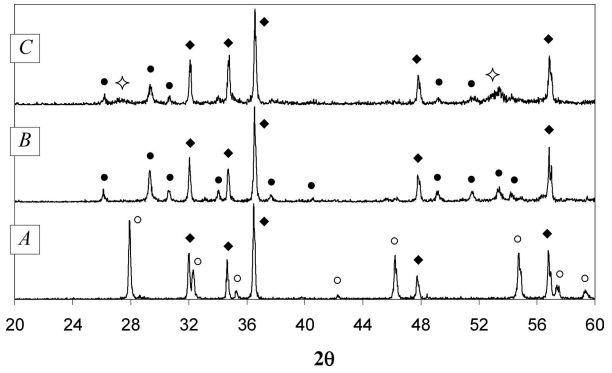

Figure 6 XRD patterns for $Zn_7Sb_2O_{12}$ spinel mixture treated at different temperatures and 0 hours soaking time. A) 500°C. B) 700°C. C) 900°C. ♦ ZnO, ○ Sb_2O_3, •Sb_2O_4, ✧ $ZnSb_2O_6$.

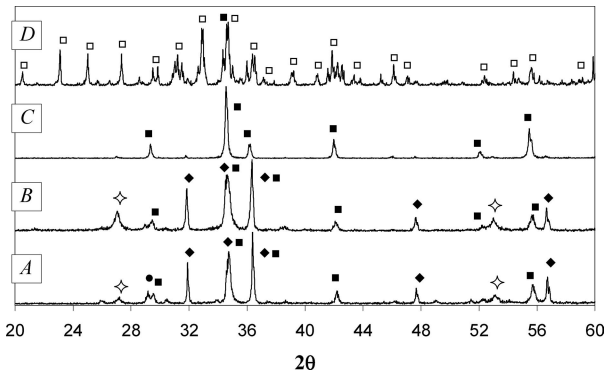

Figure 7 XRD patterns for $Zn_7Sb_2O_{12}$ spinel mixture treated at different temperatures and 4 hours soaking time. A) 500°C. B) 700°C. C) 900°C. D) 1000°C. ♦ ZnO, •Sb_2O_4, ✧ $ZnSb_2O_6$, ■ cubic $Zn_{2.33}Sb_{0.67}O_4$, □ orthorhombic $Zn_7Sb_2O_{12}$.

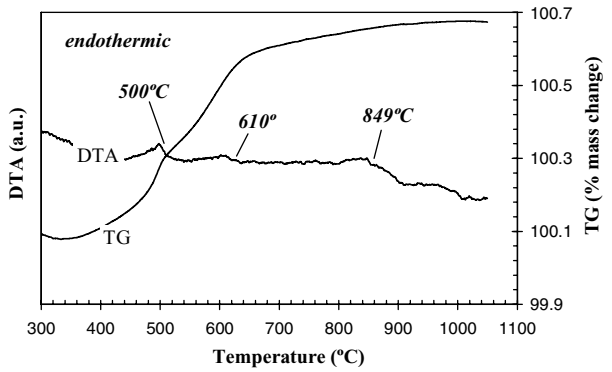

Figure 8 DTA/TG curves for composition A.

time corresponding to the complete oxidation to antimony (V); in other words the presence of zinc and bismuth oxides allows the complete oxidation of Sb (III), and this is in agree with the empirical formula of pyrochlore in which all antimony is in its oxidation state +5. XRD patterns in Fig. 4 show strong peaks of the pyrochlore phase at 530°C, together with rests of Sb_2O_4, ZnO and Bi_2O_3 still unreacted. This suggests the following reaction path: at 500°C the Sb_2O_3 first oxidizes to Sb_2O_4; this compound should stabilize the oxidation state +3 of antimony at high temperature, but in presence of ZnO and Bi_2O_3 it decomposes and starts to form the pyrochlore

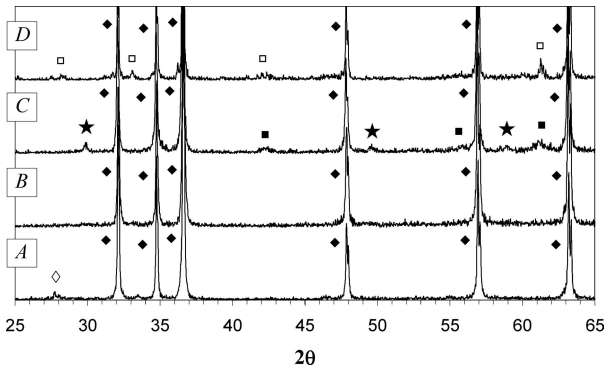

Figure 9 XRD patterns for composition A treated at different temperatures and 0 hours soaking time. A) 660°C. B) 800°C. C) 950°C. D) 1050°C. ♦ ZnO, ◊ Bi_2O_3, ⋆ $Zn_2Bi_3Sb_3O_{14}$, ■ $Zn_{2.33}Sb_{0.67}O_4$, □ $Zn_7Sb_2O_{12}$.

phase. In this way the Sb (III) can proceed with its oxidation to Sb (V) and gradually incorporates to the pyrochlore structure.

3.3. Compositions in the ZBS system

As in previous sections thermal analysis of composition A shows an exothermic peak around 500°C associated with Sb_2O_3 oxidation process. Besides, two additional exothermic reactions are also detected in this composition, one starting at 610°C and the other one at 850°C (Fig. 8). The later is followed by a gradual endothermic drop, so according to Inada it can be related to pyrochlore decomposition to form the spinel phase and liquid Bi_2O_3 (see reaction 3). XRD patterns for 0 hours thermal treatments reveal the presence of pyrochlore in composition A since 950°C, and its complete disappearance above 1050°C (Fig. 9). SEM analysis of the sample calcined at 950°C-0h shows an extremely reactive system with evidence of liquid phase (Fig. 10a, vitreous layer coating the surface). Etching the surface with acetic acid preferentially removes Bi_2O_3 and displays the existence of elongated huge structures immersed in the ZnO matrix and composed by vast accumulations of interconnected particles clearly smaller than those in the matrix (Fig. 10b and 10c). EDS analysis of marked regions in Fig. 9c indicate that such structures are richer in bismuth and antimony than the matrix, so they can be associated with great reacting blocks of pyrochlore phase (Fig. 10d).

Back to XRD analysis of composition A, heat treatments of 72 hours soaking time show the presence of $Zn_{2.33}Sb_{0.67}O_4$ spinel phase since 800°C (Fig. 11). Decomposition of pyrochlore has not yet started at this temperature therefore this spinel phase should come from the interaction between ZnO and the antimony oxide not involved in the formation of the pyrochlore (Sb/Bi > 1).

Composition B involves an increase in the amount of Bi_2O_3 as well as a decrease in that of the Sb_2O_3, with the resulting decrease in Sb/Bi ratio (Table I). As a result in DTA of composition B the intensity of the exothermic peak at 500°C related to Sb (III) oxidation is lower than in composition A (Fig. 12). Same argument explains as well the increase in intensity of the exothermic signal around 850°C corresponding to the formation of spinel phase from pyrochlore decomposition. XRD patterns and

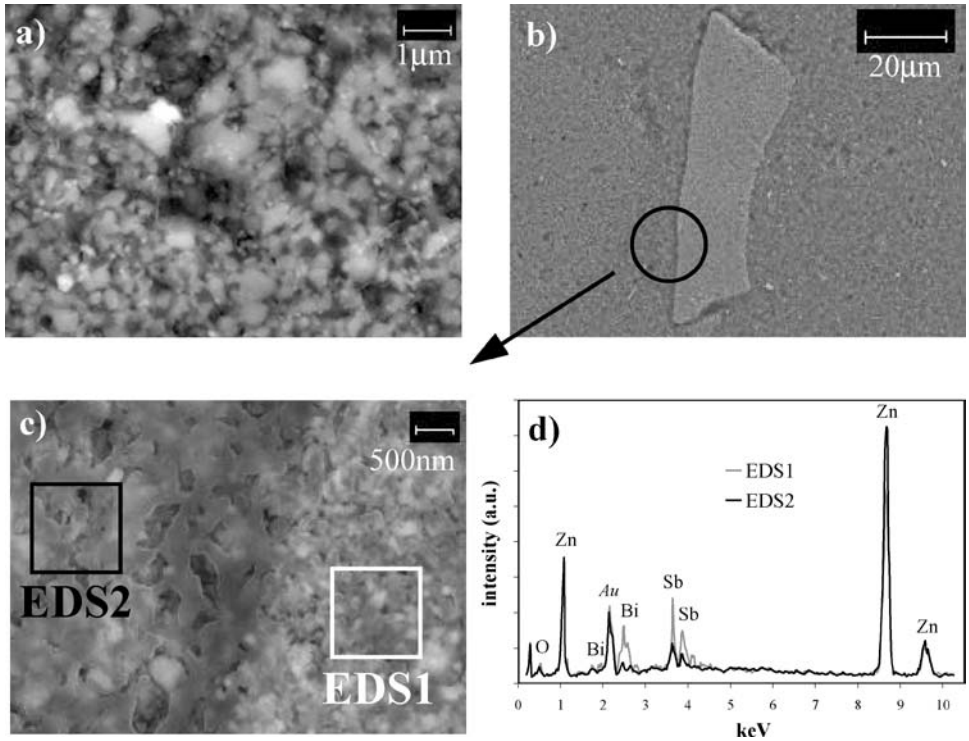

Figure 10 SEM analysis for composition A treated at 950°C−0h. a) Polished surface with evidence of liquid rests. b) Chemically etched surface showing the presence of large pyrochlore accumulations. c) Detail of the interface between the pyrochlore blocks and the ZnO matrix. d) EDS analysis of regions marked in micrograph c (see text).

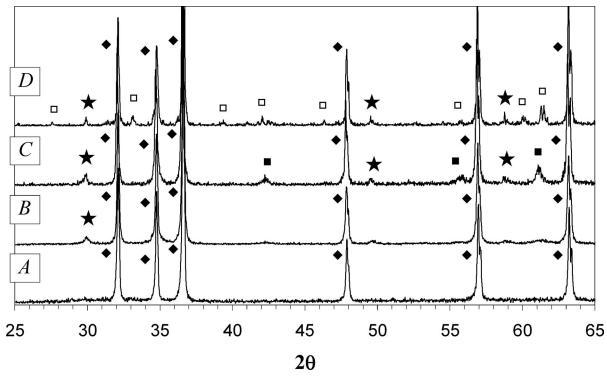

Figure 11 XRD patterns for composition A treated at different temperatures and 72 hours soaking time. A) 540°C. B) 660°C. C) 800°C. D) 950°C. ♦ ZnO, ⋆ $Zn_2Bi_3Sb_3O_{14}$, ■ $Zn_{2.33}Sb_{0.67}O_4$, □ $Zn_7Sb_2O_{12}$.

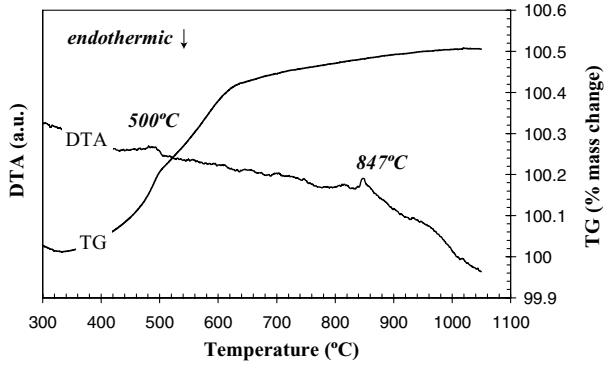

Figure 12 DTA/TG curves for composition B.

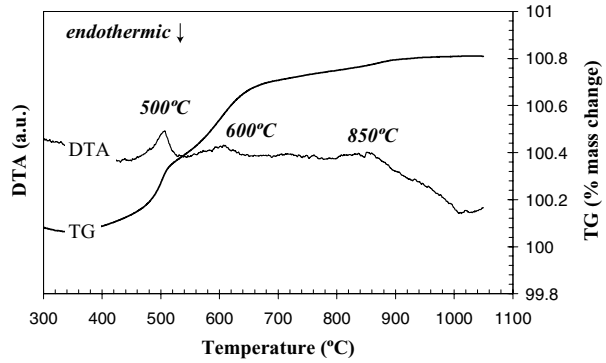

Figure 13 DTA/TG curves for composition C.

SEM analysis of composition B, non depicted here, show results quite similar to those of composition A; only the first peaks of pyrochlore phase are now detected at lower temperature, just below 600°C. The great difference in composition B is the absence in DTA of the exothermic reaction registered in composition A at 610°C (Fig. 8); since in composition A the total amount of Sb_2O_3 is greater, the presence of any exothermic signal at such temperature should then be related to the interaction in the binary ZnO-Sb_2O_3 system. Composition C will help therefore in understanding the origin of that signal at 600°C in DTA studies as it contains the highest amount of antimony oxide. In this way DTA/TG results for this composition C show again the presence of one exothermic peak around 600°C and with a higher intensity than the two other compositions (Fig. 13). XRD patterns for 0 hours heat treatments contributes again with little information, however when avoiding the kinetic restrictions, 72 hours soaking time treatments, the second reaction path that follows the Sb_2O_3 in excess (Sb/Bi = 9 in composition C) is revealed: formation around 600°C of $ZnSb_2O_6$ tri-rutile phase which above 800°C transforms into the non-stoichiometric cubic $Zn_{2.33}Sb_{0.67}O_4$ spinel phase which finally reorders above 950°C to form the stoichiometric orthorhombic $Zn_7Sb_2O_{12}$ spinel (Fig. 14). This second reaction path starts around 600°C and gives place to an exothermic signal in the thermal analysis.

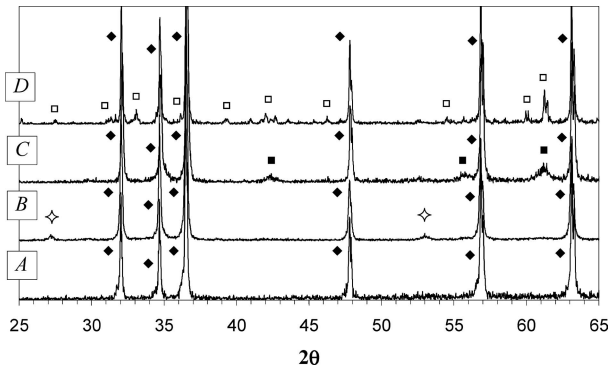

Figure 14 XRD patterns for composition C treated at different temperatures and 72 hours soaking time. A) 540°C. B) 660°C. C) 800°C. D) 950°C.♦ ZnO, ✧ $ZnSb_2O_6$, □ $Zn_{2.33}Sb_{0.67}O_4$, ■ $Zn_7Sb_2O_{12}$.

Therefore according to these results, the thermal evolution of ZBS based varistors take place through two simultaneous reaction paths: one implies the initial oxidation of antimony oxide (III) around 500°C to form Sb_2O_4. This compound reacts then with ZnO and Bi_2O_3 giving place to an intermediate pyrochlore type phase which at temperatures above 850°C decomposes to form a spinel type phase and liquid Bi_2O_3:

$$Sb_2O_3 + 1/2O_2 \overset{\sim 500^\circ C}{\longrightarrow} Sb_2O_4 \qquad (12)$$

$$3Sb_2O_4 + 4ZnO + 3Bi_2O_3 + 7/2O_2 \overset{>500^\circ C}{\longrightarrow} 2Zn_2Bi_3Sb_3O_{14} \qquad (13)$$

$$2Zn_2Bi_3Sb_3O_{14} + 17ZnO \overset{>850^\circ C}{\longrightarrow} 9Zn_{2.33}Sb_{0.67}O_4 + 3Bi_2O_3\,(liq) \qquad (14)$$

$$3Zn_{2.33}Sb_{0.67}O_4 \overset{>950^\circ C}{\longrightarrow} 3Zn_7Sb_2O_{12} \qquad (15)$$

The second reaction path takes place between the ZnO from the bulk varistor matrix and the remaining Sb_2O_3 not involved in the first reaction path

(Sb/Bi > 1). It starts again at 500°C with the oxidation of Sb (III) to Sb_2O_4 which now reacts with ZnO to form an intermediate tri-rutile type phase around 600°C. Subsequent reactions imply the transformation of this compound to the spinel phases:

$$Sb_2O_4 + ZnO + 1/2O_2 \xrightarrow{>600^\circ C} ZnSb_2O_6 \quad (16)$$

$$ZnSb_2O_6 + 6ZnO \xrightarrow{>800^\circ C} 3Zn_{2.33}Sb_{0.67}O_4 \quad (17)$$

$$3Zn_{2.33}Sb_{0.67}O_4 \xrightarrow{>950^\circ C} 3Zn_7Sb_2O_{12} \quad (18)$$

4. Conclusions

Several conclusions could be drawn from the analysis of the ZnO-Bi_2O_3-Sb_2O_3 system in the region of interest for varistors:

(1) No presence of Sb_2O_5 phase was ever detected (JCPDS Files No. 75-1567 and No. 71-587). Sb_2O_4 cervantite stabilizes the oxidation state +3 of antimony at high temperature, and only the presence of other oxides such as ZnO and Bi_2O_3 leads to further oxidation. The later represents the starting point for the two simultaneous reactions paths that govern the microstructural evolution of ZBS based varistors during sintering.

(2) $ZnSb_2O_6$ tri-rutile type phase is formed as a result of the interaction between ZnO and the remaining Sb_2O_3 (Sb/Bi > 1), but it seems not to be involved in the formation of pyrochlore from ZnO, Bi_2O_3 and Sb_2O_3, as previously reported.

(3) With a view to ZBS varistor processing, the second reaction path implies that a spinel type phase is present in the material and therefore controlling ZnO grain growth even before liquid phase sintering has started.

References

1. M. MATSUOKA, *Jpn. J. Appl. Phys.* **10** (1971) 736.
2. T. K. GUPTA, *J. Am. Ceram. Soc.* **73** (1990) 1817.
3. D. R. CLARKE, *J. Am. Ceram. Soc.* **82** (1999) 485.
4. M. INADA, *Jpn. J. Appl. Phys.* **17** (1978) 673.
5. E. OLSSON, G. DUNLOP and R. ÖSTERLUND, *J. Am. Ceram. Soc.* **76** (1993) 65.
6. M. PEITEADO, *Bol. Soc. Esp. Ceram.* V. **44** (2005) 77.
7. S. TANAKA, C. AKITA, N. OHASHI, J. KAWAI, H. HANEDA and J. TANAKA, *J. Solid State Chem.* **105** (1993) 36.
8. K. O. MAGNUSSON and S. WIKLUND, *J. Appl. Phys.* **76** (1994) 7405.
9. F. GREUTER, *Solid State Ionics* **75** (1995) 67.
10. E. OLSSON, G. L. DUNLOP and R. ÖSTERLUND, *J. Appl. Phys.* **66** (1989) 5072.
11. M. A. DE LA RUBIA, M. PEITEADO, J. F. FERNÁNDEZ and A. C. CABALLERO, *J. Eur. Ceram. Soc.* **24** (2004) 1209.
12. L. HOZER in "Semiconductor Ceramics: Grain Boundary Effects" (Polish Scientific Publishers, Warszawa, Poland, 1994) p. 44.
13. J. WONG, *J. Appl. Phys.* **46** (1975) 1653.
14. M. INADA, *Jpn. J. Appl. Phys.* **19** (1980) 409.
15. J. KIM, T. KIMURA and T. YAMAGUCHI, *J. Am. Ceram. Soc.* **72** (1989) 1390.
16. A. MERGEN and W. E. LEE, *J. Eur. Ceram. Soc.* **17** (1997) 1049.
17. J. P. GUHA, S. KUNEJ and D. SUVOROV, *J. Mater. Sci.* **39** (2004) 911.
18. J. KIM, T. KIMURA and T. YAMAGUCHI, *J. Mater. Sci.* **24** (1989) 213.
19. E. R. LEITE, M. A. L. NOBRE, E. LONGO and J. A. VARELA, *J. Mater. Sci.* **31**, (1996) 5391.
20. V. KRASEVEC, M. TRONTELJ and L GOLIC, *J. Am. Ceram. Soc*, **74** (1991) 760.
21. J. OTT, A. LORENZ, M. HARRER, E. A. PREISSNER, C. HESSE, A. FELTZ, A. H. WHITEHEAD and M. SCHREIBER, *J. Elecroceram* **6** (2001), 135.
22. K. G. V. KUMARI, P. D. VASU, V. KUMAR and T. ASOKAN, *J. Am. Ceram. Soc.* **85** (2002) 703.

Received 14 March
and accepted 28 June 2005